Available online at www.sciencedirect.com
ScienceDirect
Journal of the European Ceramic Society 27 (2007) 469–474
www.elsevier.com/locate/jeurceramsoc

Far infrared properties of sintered NiO

M.V. Nikolić [a,*], V. Blagojević [b], K.M. Paraskevopoulos [c], T.T. Zorba [c], D. Vasiljević-Radović [d], P.M. Nikolić [e], M.M. Ristić [e]

[a] *Center for Multidisciplinary Studies of the University of Belgrade, Kneza Višeslava 1, 11000 Belgrade, Serbia and Montenegro*
[b] *Faculty of Electronic Engineering, Bulevar kralja Aleksandra 72, 11000 Belgrade, Serbia and Montenegro*
[c] *Solid State Section, Physics Department, Aristotle University, 54124 Thessaloniki, Greece*
[d] *Insitute of Microelectronics and Single Crystals, Njegoševa 12, 11000 Belgrade, Serbia and Montenegro*
[e] *Institute of Technical Sciences of SASA, Knez Mihailova 35/IV, 11000 Belgrade, Serbia and Montenegro*

Available online 6 June 2006

Abstract

Far infrared reflection spectra of NiO polycrystals sintered at 1100 °C for various times (30–240 min) were measured at room temperature using a FTIR Spectrometer—Brucker 113V. The measured spectra depended on the sintering time due to differences in the microstructural morphology of the material and were compared with the NiO single crystal reflectivity diagram. Numerical analyses of the experimental spectra were performed using Kramers-Kronig analysis, a four-parameter model of coupled oscillators and the effective medium modeling theory. In the three-component effective medium model based on Bruggeman's theory we assumed the presence of pores, intergranular material and crystalline grains. The intergranular material and crystalline grains were defined as single and coupled ionic oscillators.

Keywords: Sintering; Spectroscopy; Non-destructive evaluation; Optical properties; NiO

1. Introduction

Nickel oxide (NiO) is a NaCl type antiferromagnetic oxide semiconductor with an antiferromagnetic temperature—T_N of 525 K and a partly occupied 3d lattice.[1] According to Bosman and Crevecoeur[2] appreciable conductivity in NiO could be achieved by creating Ni vacancies or by substituting Li for Ni at Ni sites. NiO has been extensively investigated. Its applications include solar selective thermal absorbers[3], electrochromic devices[4,5] positive electrodes in batteries[6] and γ-radiation dosimetry.[7] According to Patil and Kadam[8] the most attractive features of NiO include excellent durability and electrochemical stability, low material cost, it is a promising material for ion storage in terms of ion stability, has a large span optical density and can be manufactured by different techniques. Infrared reflection characterization has been proposed as a method for analyzing the quality of sintered materials.[9] A detailed analysis of IR reflection data can give useful information on the intergranular to grain ratio or on the damping coefficients that are factors related to the quality of sintered samples.

Effective medium theories have often been used to interpret the optical properties of measured spectra of microscopically inhomogeneous materials taking into account their composition and microstructural morphology.[10,11] Best known are the simple models of Maxwell-Garnett[12] or Bruggeman[13] that are based on different morphologies of the component material. The effective medium theory used to describe the dielectric function needs to take into account macroscopic volume fractions, the local microstructural geometry and microstructural topology of the analyzed material. In the case of sintered materials the simple models could not successfully explain the IR reflection spectrum, so Okamoto et al. applied a four-component effective model.[9]

In this paper we have measured and analyzed far infrared reflection spectra of NiO sintered at 1100 °C for different sintering times and compared them with the spectrum measured for single crystal NiO. Numerical analysis of the spectra was performed using Kramers-Kronig analysis,[14] a four-parameter model of coupled oscillators[15] and a three-component

* Corresponding author. Tel.: +381 11 637367; fax: +381 11 637239.
E-mail address: maria@mi.sanu.ac.yu (M.V. Nikolić).

0955-2219/$ – see front matter © 2006 Elsevier Ltd. All rights reserved.
doi:10.1016/j.jeurceramsoc.2006.04.065

effective medium model of single and coupled oscillators based on Bruggeman's model assuming the presence of pores, intergranular material and crystalline grains.

2. Experimental

Commercial NiO powder (Johnson Mathey and Co Ltd, purity 99.95%) was pressed into pellets 10 mm in diameter with a pressure of 1.5 GPa. The green density was determined as 3.724 g/cm^3. The samples were sintered in air at 1100 °C for different sintering times (30, 60, 120 and 240 min). The cooling rate was 3 °C/min. Densities of obtained samples were determined as 4.88, 5.01, 5.22 and 5.29 g/cm^3 for samples sintered 30, 60, 120 and 240 min, respectively.

The crystal structure and lattice parameters of the samples obtained were investigated using X-ray diffraction on a Philips PW 1050 diffractometer. Microstructure changes during sintering were examined using an atomic force microscope (Thermo Microscopes Auto Probe CP Research).

Room temperature far infrared and infrared reflectivity measurements were performed with near normal incidence light in the range between 60 and 1260 cm^{-1} using a Brucker 113V FTIR spectrometer. Reflectivity was measured in two ranges 60–600 and 600–1260 cm^{-1} using two different beam splitters. The measurement resolution was higher than 1 cm^{-1}. All samples were highly polished first with silicon carbide P1000 sandpaper and then with 3 μm grade diamond paste.

In order to compare with the results obtained for sintered NiO samples, we also measured far infrared and infrared reflectivity spectra for single crystal NiO prepared using the Verneuil method. Single crystal NiO freshly cleaved (1 0 0) plates were used for optical measurements.

Numerical analyses were performed using a program package developed in FORTRAN90.

3. Results and discussion

X-ray diffraction analysis confirmed that the samples sintered 60, 120 and 240 min were polycrystal single phases. Six Bragg reflections were measured between $2\theta = 10°$ and 80° and they were used to calculate lattice parameters using the least squares method. The X-ray diffractogram obtained for the sample-sintered 60 min is given in Fig. 1. Five Bragg reflections belong to a NiO cubic lattice with a NaCl space group *Fm*3*m* (JCPDS card 47-1049). The weakest Bragg reflection with $d = 2.025$ A belongs to Ni_2O_3 (JCPDS card 14-0481) with a hexagonal lattice. Its influence is small and can almost be ignored. X-ray diffraction analysis showed that the sample sintered 30 min was not a single-phase polycrystal. This is probably due to the relatively short sintering time. The reflectivity diagram measured for this sample also differed significantly from the ones obtained for longer sintering times, so it will not be considered in further analysis.

Changes in the microstructure in NiO samples with increased sintering time could also be seen in AFM images of the samples. Fig. 2 shows AFM images for samples sintered 30 and 240 min

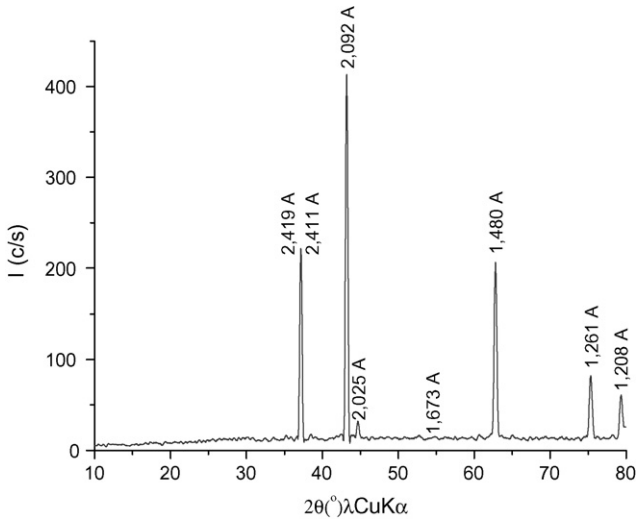

Fig. 1. X-ray diffractogram of the sample sintered 60 min.

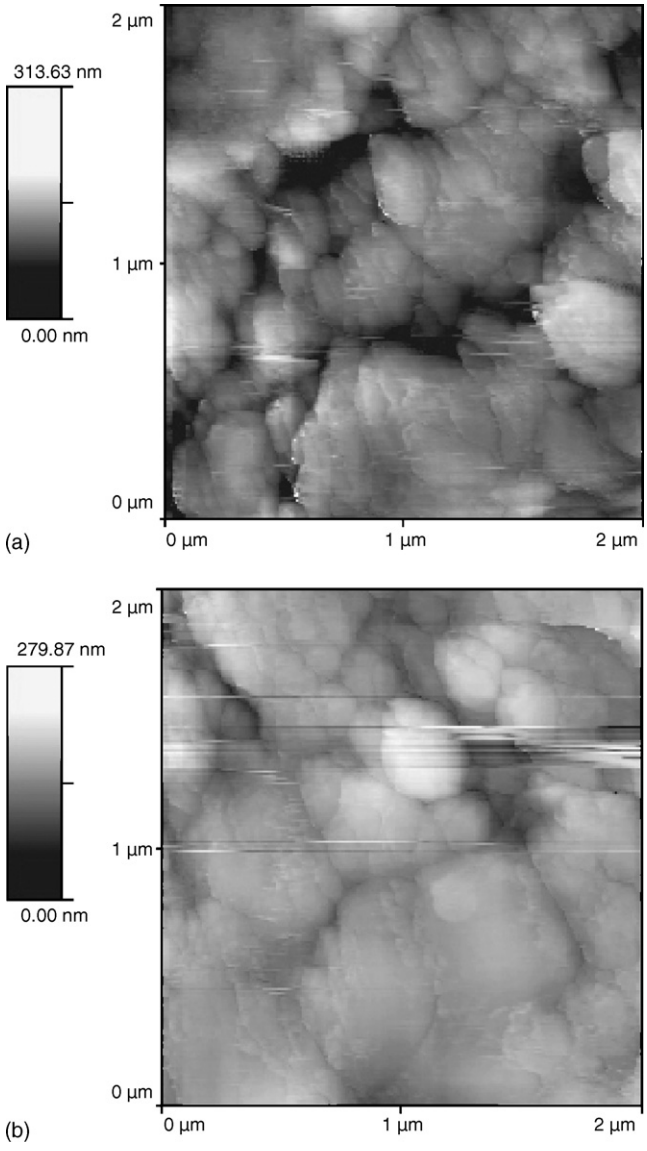

Fig. 2. AFM images of samples sintered: (a) 30 and (b) 240 min.

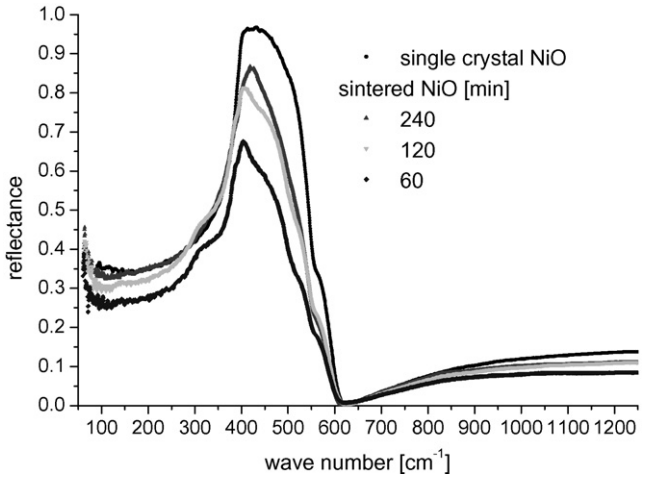

Fig. 3. FTIR reflectivity spectra for polycrystalline and single crystal samples of NiO.

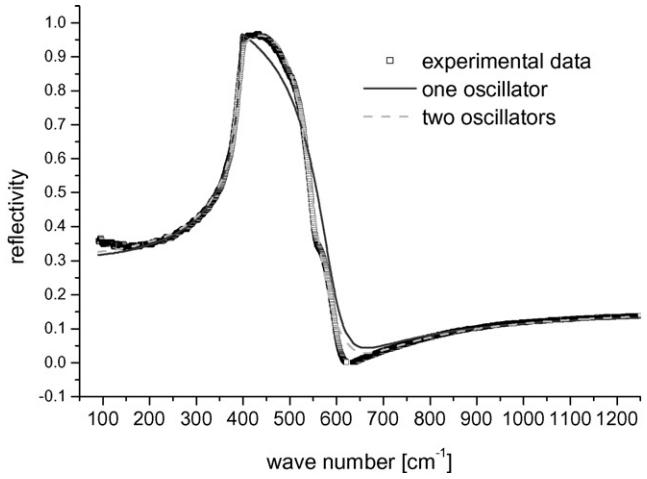

Fig. 4. Comparison of measured (points) and calculated (one oscillator—solid curve, two oscillators—dashed curve) reflection spectra for single crystal NiO.

where one can see that the grain size increased and porosity decreased with longer sintering time.

Fig. 3 shows reflectivity diagrams versus the wave number obtained for polycrystalline samples sintered for 60, 120 and 240 min and the diagram obtained for single crystal NiO. The diagram obtained for single crystal NiO has the highest main peak intensity. For polycrystalline samples the main peak intensity increases with the increase of the sintering time. The diagram obtained for the sample-sintered 240 min is the most similar to the single crystal diagram, though its main peak intensity is lower. For samples sintered 60 and 120 min one can note another sub peak—"shoulder" at frequencies below the main peak. Okamoto et al. pointed out that the main peak intensity, shape of the band and background reflection can give valuable clues regarding the quality of the sintered material.[9] The height of the main peak could reflect the growth and relative weight of crystalline grains, while the relative height of the sub peak (shoulder) could reflect the relative weight of the intergranular material, while the presence of pores reduces reflectivity.[9]

Numerical analysis of all reflectivity diagrams was first made using the Kramers-Kronig method.[14] Determination of the refractive index, n and extinction coefficient, k enabled calculation of the change of the complex dielectric permittivity and response function for all analyzed samples. The peaks of ε_2 (imaginary part of the complex dielectric function) practically correspond to positions of transversal optical modes, while maximums of the response function $\mathrm{Im}(-1/\varepsilon)$ are at the position of longitudinal modes. All mode values using the Kramers-Kronig method were used as starting parameter values for the four-parameter model of coupled oscillators and the effective medium models applied.

The reflectivity diagrams of NiO given in Fig. 3 were then numerically analyzed using the four-parameter model of coupled oscillators introduced by Gervais and Piriou.[15] The dielectric function is given as:

$$\varepsilon = \varepsilon_1 + i\varepsilon_2 = \varepsilon_\infty \prod_j \frac{\omega_{j\mathrm{LO}}^2 - \omega^2 + i\gamma_{j\mathrm{LO}}\omega}{\omega_{j\mathrm{TO}}^2 - \omega^2 + i\gamma_{j\mathrm{TO}}\omega} \quad (1)$$

where $\omega_{j\mathrm{TO}}$ and $\omega_{j\mathrm{LO}}$ are the transverse (TO) and longitudinal (LO) frequencies, $\gamma_{j\mathrm{TO}}$ and $\gamma_{j\mathrm{LO}}$ represent their damping factors and ε_∞ is the high-frequency dielectric constant. Although single crystal NiO should only have one oscillator ($\omega_{\mathrm{TO2}} \sim 394\,\mathrm{cm}^{-1}$, $\omega_{\mathrm{LO1}} \sim 601\,\mathrm{cm}^{-1}$) we obtained a better fit with two ($\omega_{\mathrm{TO1}} \sim 394\,\mathrm{cm}^{-1}$, $\omega_{\mathrm{LO1}} \sim 601\,\mathrm{cm}^{-1}$, $\omega_{\mathrm{TO2}} \sim 560\,\mathrm{cm}^{-1}$, $\omega_{\mathrm{LO2}} \sim 562\,\mathrm{cm}^{-1}$) rather than one oscillator (Fig. 4). Other authors[16,17] have also defined a "shoulder" at $\omega_{\mathrm{TO2}} \sim 560\,\mathrm{cm}^{-1}$. Pecharroman and Iglesias[17] defined the structure of NiO as a slight distortion of the $Fm3m$ NaCl structure type with this material crystallizing in space group $R\bar{3}m$, which could explain this occurrence.

The four-parameter model of coupled oscillators was also applied to analyze spectra of the sintered samples. All sintered samples had three registered ionic oscillators. The first two corresponded to the ones obtained for the single crystal. The main peak (ω_{TO1} 383–388 cm^{-1}, ω_{LO1} 582–589 cm^{-1}) was similar to the one obtained for the single crystal, though slightly shifted to lower frequencies. Compared to single crystal NiO, all sintered samples had a side band at similar frequencies to the side band of the single crystal ($\omega_{\mathrm{TO2}} \sim 560\,\mathrm{cm}^{-1}$) and another oscillator at lower frequencies (ω_{TO3} 333–400 cm^{-1}, ω_{LO3} 369–407 cm^{-1}). The origin of this oscillator could be explained using the effective medium theory.

The values calculated for high-frequency dielectric permittivity are lower for sintered samples than for single crystal NiO. They increase with the sintering time, achieving about 80% of the single crystal value (5.6) for the sample-sintered 240 min (4.25, 4.6 and 4.8 for NiO sintered 60, 120 and 240 min).

The effective dielectric function $\varepsilon_{\mathrm{eff}}$ of a heterogeneous medium can be obtained by averaging the dielectric function in each cell in the medium ε_i assuming that each cell is embedded in a homogenous medium with dielectric function ε_0.[11] For spherical cells it is reduced to the Clausius–Mossotti equation:

$$\varepsilon_{\mathrm{eff}} = \varepsilon_0 \left(\frac{1 + 2\langle\alpha\rangle}{1 - 2\langle\alpha\rangle} \right) \quad (2)$$

where ε_0 is the low-frequency dielectric constant and α is the polarizability per unit cell volume.

$$\alpha(\varepsilon_i) = \frac{\varepsilon_i - \varepsilon_0}{\varepsilon_i + 2\varepsilon_0} \tag{3}$$

The average of α taken over all cells gives:

$$\langle\alpha\rangle = \left\langle \frac{\varepsilon_i - \varepsilon_0}{\varepsilon_i + 2\varepsilon_0} \right\rangle = \sum_i \frac{\varepsilon_i - \varepsilon_0}{\varepsilon_i + 2\varepsilon_0} f_i \tag{4}$$

The Bruggeman theory regards the component materials symmetrically and imposes the self-consistency condition that $\varepsilon_{\text{eff}}(\varepsilon_0) = \varepsilon_0$, meaning $\langle\alpha\rangle = 0$. The simple model consisted of two materials embedded in an effective medium.[13] However, Okamoto et al.[9] extended this to four components, applying a so-called "four-component effective medium model" to analyze spectra of sintered SiC. Zhang et al. used this model to analyze infrared spectra of GaN films with a three-component effective medium model.[18]

In our case we defined three components:

1. Pores with volume fraction f_1 and $\varepsilon_1 = 1$. The value for volume fraction can be estimated to be the material porosity calculated from measured density values,
2. Crystalline grains with volume fraction, f_2,
3. Intergranular material with volume fraction f_3, and $f_1 + f_2 + f_3 = 1$.

In the first approximation crystalline grains and the intergranular material were defined as single ionic Lorentz oscillators:

$$\varepsilon_{2,3} = \varepsilon_{\infty 2,3} \frac{\omega^2_{j\text{LO}2,3} - \omega^2 + i\gamma_{j\text{LO}2,3}\omega}{\omega^2_{j\text{TO}2,3} - \omega^2 + i\gamma_{j\text{TO}2,3}\omega} \tag{5}$$

where $\varepsilon_{\infty 2}$ and $\varepsilon_{\infty 3}$ are the high-frequency dielectric constants of these media, $\omega_{j\text{TO}2}$, $\omega_{j\text{TO}3}$ and $\omega_{j\text{LO}2}$, $\omega_{j\text{LO}3}$ are the transverse (TO) and longitudinal (LO) frequencies, $\gamma_{j\text{TO}2}$, $\gamma_{j\text{TO}3}$, $\gamma_{j\text{LO}2}$ and $\gamma_{j\text{LO}3}$ represent their damping factors.

In this case the effective dielectric function ε_{eff} of the medium can be evaluated using the self-consistency condition:

$$\sum_{i=1}^{3} \frac{\varepsilon_i - \varepsilon_{\text{eff}}}{\varepsilon_i + 2\varepsilon_{\text{eff}}} f_i = 0 \tag{6}$$

as a root with a positive imaginary part of this third order algebraic equation at frequency ω.

As starting values of adjustable parameters (transverse and longitudinal frequencies and damping factors) for the numerical analysis we used the values obtained as a result of the four-parameter model (without the side-peak-"shoulder"). The material porosity calculated from the measured density values given was used as the volume fraction value for pores (f_1) and was a fixed parameter in the simulation. The starting value for crystalline grain volume fraction f_2 was estimated to be ~0.6 and the volume fraction for the intergranular material was calculated as $f_3 = 1 - f_1 - f_2$. The starting values of the high-frequency dielectric constant for the crystalline grains and intergranular material were set to the value obtained for single crystal NiO (5.6).

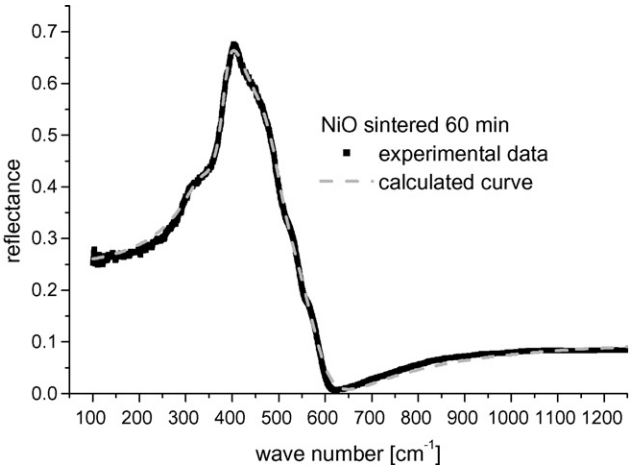

Fig. 5. Comparison of measured (points) and calculated (solid curve) reflection spectra for NiO sintered 60 min using the three-component single oscillator effective medium model.

Numerical analysis of the reflectivity diagrams given in Fig. 3 of the sintered samples was performed and relatively good agreement between measured and calculated spectra was obtained. An example is given in Fig. 5 for the sample sintered 60 min. The crystalline grain phonon mode frequencies obtained for all sintered samples were $\omega_{\text{TO}2} \sim 383\ \text{cm}^{-1}$ and $\omega_{\text{LO}2} \sim 592\ \text{cm}^{-1}$. Compared to the values obtained for single crystal NiO (the ones we calculated and literature data[16,17]) these values have slightly shifted to lower frequencies. The intergranular material phonon mode frequencies varied for different sintering times. They were in the range $\omega_{\text{TO}3}$ 280–299 cm^{-1}, $\omega_{\text{LO}3}$ 370–497 cm^{-1}. Table 1 contains the values determined for volume fractions. Volume fraction of crystalline grains increased with the sintering time, while the volume fraction for the intergranular material decreased and was quite low for the sample sintered for 240 min.

Even though application of the previously effective medium model gave very good agreement between measured and calculated spectra we defined a three-component effective medium model where the crystalline grains and intergranular material could be modeled with two coupled oscillators according to the definition given in Eq. (1). The reason for this was the fact that three coupled oscillators were defined for all sintered NiO samples using the four-component coupled oscillator model and better fitting of the side band at lower frequencies could be attempted, especially as this band was more pronounced for the samples sintered for shorter times indicating it to be a measure

Table 1
Parameter values determined from fitting effective medium models to measured IR reflection spectra of NiO samples sintered for different times

Sintered time	Single oscillator			Coupled oscillators		
	f_1	f_2	f_3	f_1	f_2	f_3
60	0.241	0.603	0.156	0.241	0.572	0.187
120	0.209	0.653	0.138	0.209	0.612	0.179
240	0.199	0.746	0.055	0.199	0.709	0.092

Table 2
Parameter values determined from fitting the three-component coupled oscillator effective medium model to measured IR spectra of NiO samples sintered for different times, $\omega_{TO2} \sim 385\,cm^{-1}$ and $\omega_{LO2} \sim 596\,cm^{-1}$

S.t.	$\varepsilon_{2\infty}$	γ_{2LO}	γ_{2TO}	$\varepsilon_{3\infty}$	ω_{31LO}	γ_{31LO}	ω_{31TO}	γ_{31TO}	ω_{32LO}	γ_{32LO}	ω_{32TO}	γ_{32TO}
60	3.48	44.4	27.7	21.2	520.4	128.3	422.9	178.2	373.2	54.0	316.1	51.8
120	3.87	28.4	22.9	21.8	512.1	146.0	397.7	29.6	396.9	41.1	304.5	50.2
240	5.51	44.7	22.0	8.35	488.1	156.6	402.6	80.1	435.5	37.4	307.1	70.2

s.t. denotes the sintering time.

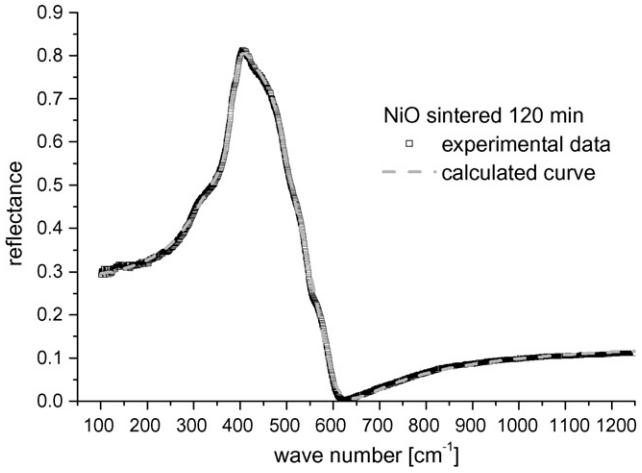

Fig. 6. Comparison of measured (points) and calculated (solid curve) reflection spectra for NiO sintered 120 min using the three-component coupled oscillator effective medium model.

of higher structural disorder. Zhang et al.[18] and Okamoto et al.[9] also proposed modeling of the intergranular material with more than one oscillator as appropriate for a more detailed study of intergranular materials. As starting parameters we used a combination of values obtained using the single oscillator effective medium model and the four-component coupled oscillator model. Very good agreement between calculated and measured spectra was obtained in the case when the crystalline grains were modeled with one and the intergranular material with two coupled oscillators (Fig. 6). In this case the values obtained for volume fractions for crystalline grains were slightly lower and thus for the intergranular material slightly higher (Table 1), accounting for the better fit with higher participation of the intergranular material. The values obtained for crystalline grain phonon frequencies were similar to the ones obtained for the single oscillator effective medium model $\omega_{TO2} \sim 385\,cm^{-1}$ and $\omega_{LO2} \sim 596\,cm^{-1}$. Table 2 gives all the remaining parameter values obtained. The intergranular material phonon mode frequencies varied for different sintering times. Their coupling enabled very good agreement between calculated and experimental data.

4. Conclusion

In conclusion, a detailed analysis was made of far infrared reflection spectra of NiO polycrystals sintered for different times. The measured spectra were modeled using Kramers-Kronig analysis, followed by the four-component model of coupled oscillators. The parameter values obtained were used as starting parameters for effective medium modeling. A three-component single oscillator model effective medium model based on the self-consistency condition assuming the presence of pores, crystal grains and intergranular material gave relatively good agreement between experimental and calculated curves, but the best results were obtained when the intergranular material was modeled as two coupled oscillators. This leads us to the conclusion that infrared spectroscopy can be a very powerful and non-destructive method for the characterization of materials with complex microstructures.

Acknowledgements

The authors would like to express their gratitude to Prof. S. Đurić for X-ray diffraction analysis. This work was performed as part of projects 1832 and 6150 financed by the Ministry for Science and Environmental Protection of the Republic of Serbia.

References

1. Kunz, A. B., Electronic structure of NiO. *J. Phys. C.: Solid State Phys.*, 1981, **14**, L455–L460.
2. Bosman, A. J. and Crevecoeur, C., Mechanism of the electrical conduction in Li-doped NiO. *Phys. Rev.*, 1966, **144**, 763–770.
3. Cook, J. G. and Koffyberg, F. P., Solar thermal absorbers employing oxides of Ni and Co. *Solar Energy Mater.*, 1984, **10**, 55–67.
4. Lampert, C. M., Electrochromic materials and devices for energy efficient windows. *Solar Energy Mater.*, 1984, **11**, 1–27.
5. Hale, J. S., DeVries, M., Dworak, B. and Woollam, J. A., Visible and infrared optical constants of electrochromic materials for emissivity modulation applications. *Thin Solid Films*, 1998, **313/314**, 205–209.
6. Vincent, C. A., Bonion, F., Lizzari, M. and Scrosati, B., *Modern batteries* (*1st ed.*). Edward Arnold, London, 1987.
7. Arshak, K., Korostynska, O. and Harris, J., γ-radiation dosimetry using screen printed nickel-oxide thick films. In *Proceedings of the 23rd International Conference on Microelectronics, MIEL 2002*, 2002.
8. Patil, P. S. and Kadam, L. D., Preparation and characterization of spray pyrolyzed nickel oxide (NiO) films. *Appl. Surf. Sci.*, 1999, **211–221**, 2000.
9. Okamoto, Y., Ordin, S. V., Kawara, T., Fedorov, M. I., Miida, Y. and Miyakawa, T., Infrared-reflection characterization of sintered SiC thermoelectric semiconductors with the use of a four-component effective medium model. *J. Appl. Phys.*, 1999, **85**, 6728–6737.
10. MacMillan, M. F., Devaty, R. P., Choyke, W. J., Goldstein, D. R., Spanier, J. E. and Kurtz, A. D., Infrared reflectance of thick p-type porous SiC layers. *J. Appl. Phys.*, 1996, **80**, 2412–2419.
11. Spanier, J. E. and Herman, I. P., Use of hybrid phenomenological and statistical effective-medium theories of dielectric functions to model the infrared reflectance of porous SiC films. *Phys. Rev. B*, 2000, **61**, 437–450.

12. Maxwell-Garnett, J. C., Colours in metal glasses and in metallic films. *Philos. Trans. R. Soc. London A*, 1904, **203**, 385–420.
13. Bruggeman, D. A. G., Berechnung verschiedener physikalischer konstanten von heterogenen substanzen. *Ann. Phys. (Leipzig)*, 1935, **24**, 636–679.
14. Roessler, D. M., Kramers-Kronig analysis of reflection data. *Brit. J. Appl. Phys.*, 1965, **16**, 1119–1123.
15. Gervais, F. and Piriou, B., Temperature dependence of transverse- and longitudinal-optic modes in TiO_2 (rutile). *Phys. Rev. B*, 1974, **10**, 1642–1654.
16. Gielisse, P. J., Plendl, J. N., Mansur, L. C., Marshall, R., Mitra, S. S., Mykolajewycz, R. and Smakula, A., Infrared properties of NiO and CoO and their mixed crystals. *J. Appl. Phys.*, 1965, **36**, 2446–2450.
17. Pecharroman, C. and Iglesias, J. E., A method for the determination of infrared optical constants from reflectance measurements on powdered samples. *J. Phys. Condens. Matter*, 1994, **6**, 7125–7141.
18. Zhang, X., Hou, Y.-T., Feng, Z.-C. and Chen, J.-L., Infrared reflectance of GaN films grown on Si(0 0 1) substrates. *J. Appl. Phys.*, 2001, **89**, 6165–6170.